POLITECNICO
MILANO 1863

SCUOLA DI INGEGNERIA INDUSTRIALE
E DELL'INFORMAZIONE

Executive Summary of the Thesis

Study of Heliocentric Escape Dynamics from Earth-Moon L2 Near Rectilinear Halo Orbits

Laurea Magistrale in Space Engineering - Ingegneria Spaziale

Author: Francesca Giulia Cicchi

Advisor: Prof. Camilla Colombo

Co-advisor: Mathilda Bolis

Academic year: 2024-2025

1. Introduction

The growing interest in Moon exploration is expected to increase the number of spacecraft operating in the cislunar region over the next decades. In this context, Near-Rectilinear Halo Orbits (NRHOs) have gained particular importance, since their geometry allows long visibility windows from Earth, limited eclipse periods, and moderate station-keeping costs. For these reasons, NRHOs have been selected as the reference orbit for the Lunar Gateway within the Artemis program. As more missions adopt this orbits, the long-term sustainability of this environment becomes a relevant issue.
As in near-Earth space, inactive spacecraft can accumulate and create operational risks, motivating the extension of debris mitigation principles to the cislunar domain. For spacecraft in this region, the main End-of-Life (EoL) options are: heliocentric disposal, lunar impact, Earth re-entry, and transfer to a lunar graveyard orbit. Among these strategies, heliocentric disposal is generally preferred, as it allows the spacecraft to permanently leave the Earth-Moon system.
Previous studies [1] have investigated heliocentric disposal from NRHOs within the Bicircular Restricted Four-Body Problem (BCR4BP) framework. One of the main findings is that the relative Sun-Earth-Moon configuration is a key factor influencing the success of escape from the Earth-Moon region. However, this geometric dependence has not been investigated within a systematic parametric analysis, and the dynamical reasons behind the different escape behaviours remain only partially understood. These gaps motivate the present study.
This thesis aims to answer the following research questions:

- How does the relative Sun-Earth-Moon configuration influence heliocentric escape from Earth-Moon L_2 NRHOs?
- Can the escape behaviour be interpreted in terms of the dynamical structures governing transport in the coupled system?

To address these questions, the coupled Circular Restricted Three-Body Problem (CR3BP) formulation is adopted and heliocentric disposal trajectories are generated using invariant manifolds associated with representative NRHOs, framework already proposed by Bolis et al. [2]. A parametric study is carried out by varying both the orbital phase angle along the NRHO and the Sun-Earth-Moon configuration in different time instants. The results are summarised through escape maps, which identify successful disposal regions and dynamically sensitive areas. The escape behaviour is finally interpreted using energetic and stability indicators.

2. Dynamical model

The CR3BP is a fundamental model in astrodynamics used to study the motion of a small body under the gravitational influence of two massive primaries that follow circular orbits around their common centre of mass [3]. In this framework, the third body, typically the spacecraft, is assumed to have negligible mass compared to the primaries, such that its motion does not affect the dynamics of the two primary bodies. The problem is formulated in a rotating reference frame in which the two primaries lie in the x-axis. This frame rotates with constant angular velocity and completes a right-handed coordinate system. The equations of motion (EOMs) in this frame are:

$$\begin{cases} \ddot{x} - 2\dot{y} = \dfrac{\partial U}{\partial x} \\ \ddot{y} + 2\dot{x} = \dfrac{\partial U}{\partial y} \\ \ddot{z} = \dfrac{\partial U}{\partial z} \end{cases} \tag{1}$$

where the pseudo-potential function $U(x, y, z)$ is defined as:

$$U(x, y, z) = \frac{1}{2}(x^2 + y^2) + \frac{1-\mu}{r_1} + \frac{\mu}{r_2} \tag{2}$$

All quantities are expressed in dimensionless form. Lengths are scaled by the average distance between the two primaries, while time is scaled such that the angular velocity of the rotating frame is equal to one. In this configuration, the larger primary is located at $x = -\mu$, while the smaller primary is located at $x = 1-\mu$, where μ denotes the dimensionless mass parameter of the system. Its value depends on the considered system: in the Earth-Moon case $\mu = 0.01215$, while in the Sun-Earth system $\mu = 3.0404 \times 10^{-6}$. This normalisation simplifies the EOMs and allows a consistent description of different three-body systems within the same mathematical framework. The distances between the spacecraft and the two primaries are denoted by r_1 and r_2, respectively, and can be expressed as:

$$r_1 = \sqrt{(x+\mu)^2 + y^2 + z^2} \tag{3}$$

$$r_2 = \sqrt{(x-1+\mu)^2 + y^2 + z^2} \tag{4}$$

Within the CR3BP, only one integral of motion exists, known as the Jacobi Constant (JC). It is defined as:

$$JC = 2U - V^2 \tag{5}$$

where $V^2 = \dot{x}^2 + \dot{y}^2 + \dot{z}^2$ represents the squared magnitude of the velocity in the rotating reference frame. According to this definition, higher values of JC correspond to lower values of the spacecraft energy. For a given value of the JC, the motion of the spacecraft is confined by this energy constraint. Since the squared velocity must be non-negative, the condition $V^2 \geq 0$ implies that only regions where $U \geq JC/2$ are dynamically accessible. The boundary between allowed and forbidden regions is defined by the Zero-Velocity Surfaces (ZVSs). In the planar case, these reduce to Zero-Velocity Curves (ZVCs), which provide a convenient two-dimensional representation of the admissible regions of motion. The topology of the ZVCs strongly depends on the value of the JC and determines whether the neck regions around the collinear Lagrange points are open or closed.

2.1. Disposal framework

In this work, the CR3BP is applied to both the Earth-Moon and the Sun-Earth systems in a coupled manner, in order to describe trajectories that evolve from the cislunar region toward the heliocentric environment [4]. The spacecraft dynamics are propagated in the Earth-Moon CR3BP when the motion is dominated by the gravitational interaction of the Earth and the Moon. As the trajectory moves away from the cislunar region, the relative influence of the Sun increases and the propagation is performed within the Sun-Earth CR3BP. The transition between the two formulations is based on the definition of prevalence regions, which identify the spatial domains where one restricted three-body model provides a better local approximation of the Sun-Earth-Moon system than the other. These regions depend on the relative configuration of the primaries and vary with time. The two rotating reference frames are related by a relative rotation angle α, which fully characterises their instantaneous orientation. This angle evolves in time according to the difference between the angular velocities of the Earth-Moon and Sun-Earth synodic frames. When the trajectory crosses the prevalence boundary, the spacecraft state is transformed between the corresponding rotating frames, including both position and velocity components. This mapping ensures a consistent description of the dynamics within the coupled CR3BP framework. Fig. 1 shows the relation between the two rotating reference frames.

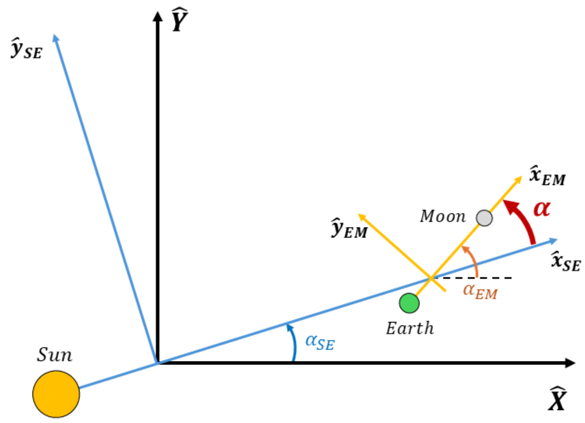

Figure 1: Relation between the Sun-Earth and Earth-Moon rotating frames.

3. Halo orbits and invariant Manifolds

This section outlines the numerical approach used to compute the Earth-Moon L_2 halo orbit family and to identify the NRHO subset adopted in the disposal analysis. Halo orbits are three-dimensional periodic solutions of the CR3BP that exist in the vicinity of the collinear libration points. In the Earth-Moon system, the L_2 halo family spans a wide range of geometries, from nearly planar motions close to the Lyapunov orbit to strongly three-dimensional trajectories that extend towards the lunar region.

Periodic halo orbits are obtained by exploiting the symmetry of the CR3BP equations with respect to the xz-plane. Periodicity is enforced by requiring an orthogonal crossing of the xz-plane at half-period. Starting from an initial guess, a differential correction scheme iteratively updates the initial conditions until the symmetry conditions at the next plane crossing are satisfied within a prescribed tolerance. In this procedure, the State Transition Matrix (STM) is used to relate variations in the initial state to variations at the final state.

To generate the full halo family, numerical continuation is applied. Successive periodic solutions are obtained by using a converged orbit as the initial guess for a nearby one, while progressively varying a selected initial parameter. In this work, starting from an orbit approximately in the middle of the family, continuation is performed along two branches of the family: one towards the Moon, mainly driven by variations in x_0, and one towards the L_2 point, where variations in z_0 become more relevant.

NRHOs are identified as a specific subset of the halo family based on their linear stability properties. In the L_2 Earth-Moon framework, this definition corresponds to halo orbits that approach the Moon and have a perilune radius approximately between 1832 km and 17390 km [5]. Within this range, the orbits are linearly stable or only weakly unstable, which makes them suitable for long-duration missions. The stability properties are described by the stability index:

$$\nu_{\max} = \frac{1}{2}\left(\|\lambda_{\max}\| + \frac{1}{\|\lambda_{\max}\|}\right) \tag{6}$$

where $\lambda_{\max}$ is the nontrivial eigenvalue of maximum modulus of the monodromy matrix, defined as the STM evaluated over one orbital period. Linearly stable orbits have $\nu_{\max} = 1$, while unstable orbits have $\nu_{\max} > 1$.

3.1. Candidates for the analysis

The escape analysis is carried out on four representative L_2 NRHOs, selected to capture different dynamical regimes within the NRHO subset. The main parameters of the selected orbits are summarised in Tab. 1, while their three-dimensional geometry in the rotating frame is shown in Fig. 2.

JC [-]	SI [-]	r_p [km]	T [days]
3.0546	1.0962	2 184.13	6.1427
3.0474	1.2971	3 106.97	6.5193
3.0271	1.6908	7 932.02	8.0206
3.0176	1.0944	12 996.74	9.3312

Table 1: Parameters of the NRHOs selected for the escape analysis.

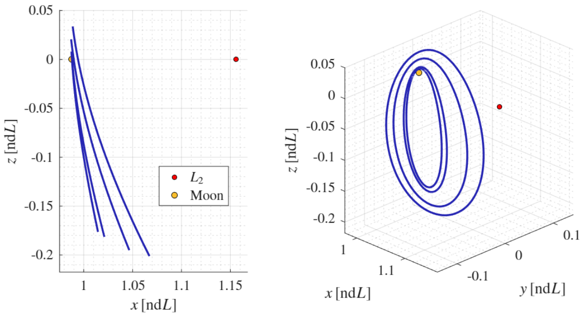

Figure 2: Selected NRHOs.

The selected cases cover different stability and geometrical properties. One of the orbits considered is characterised by the lowest linear stability in the NRHO range. A second orbit corresponds to the configuration selected for the Lunar Gateway mission and is considered due to its operational relevance. The remaining two orbits exhibit similar SI values but significantly different perilune radii. These configurations are selected to investigate how the escape dynamics evolve along the NRHO family.

For each selected NRHO, the associated invariant manifolds are computed in order to generate natural escape trajectories. In the CR3BP, unstable periodic orbits admit stable and unstable invariant manifolds that guide the motion away from or towards the orbit.

Let $\mathbf{\Lambda}^u(\theta_0)$ denote the unstable eigenvector of the monodromy matrix at a reference point of the periodic orbit. The corresponding direction at a generic phase θ along the orbit is obtained through the STM as

$$\mathbf{\Lambda}^u(\theta) = \mathbf{\Phi}(t_0, t)\, \mathbf{\Lambda}^u(\theta_0) \tag{7}$$

The eigenvector is then normalised, and the corresponding unit vector is denoted by $\hat{\mathbf{\Lambda}}^u(\theta)$. A small perturbation ε is applied along this direction to generate the initial conditions of the unstable manifold:

$$\mathbf{x}_0^u(\theta) = \mathbf{x}_0(\theta) \pm \varepsilon\, \hat{\mathbf{\Lambda}}^u(\theta) \tag{8}$$

The perturbed states are subsequently propagated forward in time, generating the unstable manifold branches that depart from the NRHO and are used in the escape analysis.

4. Escape Analysis

Heliocentric escape is investigated by propagating unstable manifold trajectories within the coupled CR3BP framework. Two parametric analyses are performed by varying θ, the phase angle along the NRHO, and:

- in the first case, α_0, representing the initial Sun-Earth-Moon configuration at the beginning of the propagation,
- in the second case, α_{cross}, representing the configuration at the instant in which the spacecraft first enters the Sun's sphere of influence.

Both parameters are discretised with a resolution of 1°. For each pair (θ, α), both manifold branches are analysed by applying positive and negative perturbations along the unstable direction. Each trajectory is propagated for up to 10 months, this long time window is adopted to capture late escape events and long-term bounded behaviour. Depending on their evolution, trajectories are classified into five possible outcomes:

- Escape through Sun-Earth L_1
- Escape through Sun-Earth L_2
- Earth impact
- Moon impact
- No escape

Escape through L_1 or L_2 requires both a geometrical and an energetic condition. The geometrical condition requires that the trajectory must cross the corresponding Lagrange point location. An energetic consistency condition is also imposed:

$$V^2 - \Delta JC > 0, \tag{9}$$

where ΔJC is defined as the difference between the JC of the considered Lagrange point and that of the trajectory in the Sun-Earth system. This condition ensures that the trajectory lies in a dynamically accessible region beyond the closed ZVC associated with the corresponding Lagrange point.

5. Results

The orbit with $JC = 3.0271$ and $SI = 1.6908$ is selected as reference case, as it is characterised by the highest instability among the considered NRHOs. The escape map as a function of θ and α_0 for positive ε is shown in Fig. 3, where $\theta = 0°$ corresponds to the apolune.

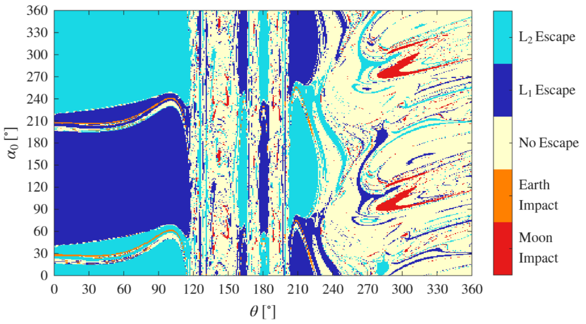

Figure 3: Escape map in (θ, α_0).

The escape map reveals a clear dynamical organisation characterised by the coexistence of regular and highly sensitive regions. Extended domains of direct escape are observed for specific intervals of the phase angle θ, where small variations of the initial configuration lead to the same final outcome. In contrast, a central band exhibits a fragmented structure, where neighbouring initial conditions may produce qualitatively different behaviours. This sensitivity reflects the nonlinear nature of the dynamics and the influence of close lunar interactions. When the map is reformulated as a function of α_{cross}, as shown in Fig. 4, the overall organisation remains similar.

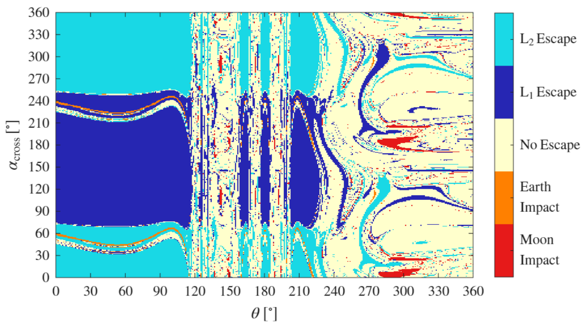

Figure 4: Escape map in $(\theta, \alpha_{\text{cross}})$.

However, the separation between escape through L_1 and L_2 appears more clearly organised. This indicates that the specific escape path is strongly influenced by the Sun-Earth-Moon configuration at the first transition into the Sun-Earth dynamical regime for geometrical reasons. To further characterise the dynamical behaviour within this framework, representative trajectories corresponding to different outcomes are presented and analysed, highlighting the variety of possible dynamical evolutions. These escape maps are therefore relevant not only from an operational perspective, as they highlight favourable configurations for heliocentric disposal, but also from a dynamical standpoint, providing a consistent basis for further investigations.

5.1. JC and FTLE

To gain further insight into the mechanisms governing escape, the JC and the Finite-Time Lyapunov Exponent (FTLE) are analysed for the reference orbit.

The evolution of the JC is analysed along the propagated manifolds. This is particularly relevant in the present multi-frame framework, where the value of the JC depends on the active dynamical model. By examining the JC in the Sun-Earth frame, it is observed that trajectories leading to escape generally exhibit lower JC values already at their first entrance into the Sun-Earth region. Indeed, it is reasonable to expect that trajectories entering the Sun-Earth region with lower JC values are more likely to escape, as they are associated with more open ZVCs. Motivated by this observation, a JC map is constructed by evaluating the Jacobi constant at the first transition as a function of α_0 and θ as shown in Fig. 5.

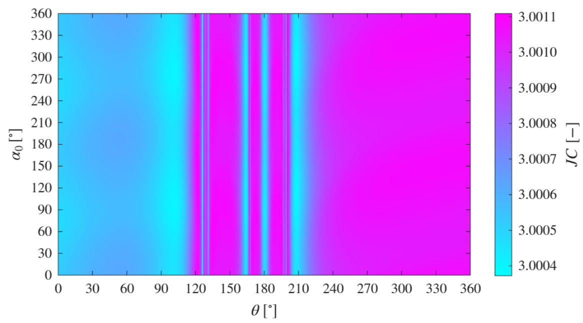

Figure 5: JC evaluated in the Sun-Earth system at the first switching as a function of α_0 and θ.

The resulting structure is consistent with the escape map previously discussed: regions characterised by lower JC values correspond predominantly to direct escape configurations.

The FTLE is analysed as an indicator of local dynamical sensitivity along the unstable manifolds. The FTLE, here denoted by $\sigma_{T_{ref}}$, is computed from the Cauchy-Green deformation tensor, defined as $\mathbf{C} = \mathbf{\Phi}^{\mathrm{T}}\mathbf{\Phi}$, where $\mathbf{\Phi}$ is the STM evaluated at time $T_{ref} = t - t_0$. It is given by

$$\sigma_{T_{ref}} = \frac{1}{|T_{ref}|} \ln \lambda_{\max}\left(\sqrt{\mathbf{C}}\right) \qquad (10)$$

where $\lambda_{\max}(\cdot)$ denotes the maximum eigenvalue. In this analysis, T_{ref} is set equal to one day. By examining the FTLE evolution along the propagated manifolds, it is observed that trajectories leading to escape tend to exhibit lower FTLE values once they enter the Sun-Earth frame, whereas non-escaping trajectories display more irregular and higher values. Motivated by this behaviour, an FTLE map is constructed by evaluating this parameter at the first switching instant as a function of α_0 and θ as shown in Fig. 6.

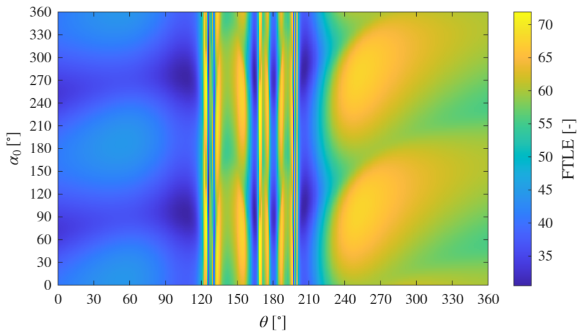

Figure 6: FTLE evaluated in the Sun-Earth system at the first switching as a function of α_0 and θ.

The resulting structure is consistent with the escape regions previously identified: lower FTLE values seem to be predominantly associated with direct escape configurations, while higher values correspond to bounded motion or impact cases.

6. Conclusions

This work provides a structured analysis of heliocentric disposal from Earth-Moon L_2 NRHOs within the coupled CR3BP framework. Through a parametric study, it has been shown that the success of escape strongly depends on both the orbital phase along the NRHO and the relative Sun-Earth-Moon configuration. The escape maps reveal the coexistence of robust escape regions and highly sensitive domains. Despite this complexity, different patterns emerge, allowing the identification of favourable configurations for disposal. The analysis of the JC and the FTLE at the first transition into the Sun-Earth region further clarifies the mechanisms governing escape. Lower JC values are associated with energetic accessibility of the gateway, while reduced FTLE values indicate lower local dynamical sensitivity. Their combined behaviour provides additional insight into the conditions leading to successful heliocentric escape and indicates that JC and FTLE evaluated at the first transition can act as early predictive tools, reducing the need for full long-term propagation. Overall, the results contribute to a more systematic understanding of heliocentric disposal from NRHOs and provide a useful dynamical basis for the preliminary design of EoL strategies in the cislunar environment.

7. Acknowledgements

I would like to thank my advisor Prof. Camilla Colombo for her guidance and my co-advisor Mathilda Bolis for her support throughout this work.

References

[1] Kenza Katiane Boudad. Disposal dynamics from the vicinity of near rectilinear halo orbits in the earth-moon-sun system. Master's thesis, Purdue University, 2018.

[2] Mathilda Bolis, Elisa M Alessi, Camilla Colombo, et al. End-of-life disposal design for near-rectilinear halo orbits. In *76th International Astronautical Congress (IAC 2025)*, pages 1–14, 2025.

[3] Victory Szebehely. *Theory of orbit: The restricted problem of three Bodies.* Elsevier, 1967.

[4] Roberto Castelli. On the relation between the bicircular model and the coupled circular restricted three-body problem approximation. In *Nonlinear and Complex Dynamics: Applications in Physical, Biological, and Financial Systems*, pages 53–68. Springer, 2011.

[5] Emily M Zimovan-Spreen, Kathleen C Howell, and Diane C Davis. Near rectilinear halo orbits and nearby higher-period dynamical structures: orbital stability and resonance properties. *Celestial Mechanics and Dynamical Astronomy*, 132(5):28, 2020.